Processing of Single Channel Air and Water Gun Data for Imaging an Impact Structure at the Chesapeake Bay

Myung W. Lee

U.S. Geological Survey Bulletin 2169

U.S. Department of the Interior
U.S. Geological Survey

U.S. Department of the Interior
Bruce Babbitt, Secretary

U.S. Geological Survey
Charles G. Groat, Director

This report is only available on-line at:
http://greenwood.cr.usgs.gov/pub/bulletins/b2169/index.html

Published in the Central Region, Denver, Colorado
Manuscript approved for publication July 28, 1999
Graphics by the author and Gayle M. Dumonceaux
Photocomposition by Gayle M. Dumonceaux
Edited by Lorna Carter

Contents

Abstract 1
Introduction 1
Acknowledgments 1
Data Processing 1
    Air Gun (GI Gun) Data 1
        Static Correction and Direct Arrival Correction 1
        Gain, Deconvolution 1
        Wavelet Deconvolution and Matched Filtering 2
        F-X Deconvolution 4
    Water Gun Data 4
Discussion 5
Summary 7
References Cited 7

Figures

1. Location map of the single channel seismic lines in Chesapeake Bay 2
2. Processing flowchart 2

3–7. Images showing:

3. Examples of seismic data processing 3
4. Effect of signal enhancement filter (F-X deconvolution) 4
5. Wavelet deconvolution for the water gun data 5
6. Result of water gun data processing 6
7. Final processing for line 7, acquired by GI (air) gun 6

Processing of Single Channel Air and Water Gun Data for Imaging an Impact Structure at the Chesapeake Bay

By Myung W. Lee

Abstract

Processing of 20 seismic profiles acquired in the Chesapeake Bay area aided in analysis of the details of an impact structure and allowed more accurate mapping of the depression caused by a bolide impact. Particular emphasis was placed on enhancement of seismic reflections from the basement. Application of wavelet deconvolution after a second zero-crossing predictive deconvolution improved the resolution of shallow reflections, and application of a match filter enhanced the basement reflections. The use of deconvolution and match filtering with a two-dimensional signal enhancement technique (F-X filtering) significantly improved the interpretability of seismic sections.

Introduction

In 1996, a single channel seismic data set was acquired in the Chesapeake Bay area, near Norfolk, Virginia, using a generator injector (GI) air gun and a water gun. The purpose of the data acquisition was to accurately map the impact structure by resolving the basement surface, the basement structure, internal disruptions in stratigraphy, and possible faulting. These lines were shot around the impact structure, supplementing the existing regional seismic lines in the area. The majority of these data (19 lines) were acquired using a GI gun (45 $in.^3$ generator chamber and 45 $in.^3$ injector chamber) with a 50-m long recording streamer; lines 13a and 15a were shot with a 15 $in.^3$ water-gun and a solid-element streamer about 4.5 m long. Line locations are shown in figure 1.

Important processing considerations were as follows: (1) For the GI gun data, the distance from gun to streamer center is generally much greater than the water depth, so it will be hard to image the shallow section due to interference between reflection and direct arrival. (2) Gas emanating from sediments was obvious in many places, and its presence was confirmed with a high-frequency system (chirp sonar). In areas where gas was present, the quality of the section was locally degraded by the frequency shift of the reflections, strong reverberations and "time sag." (3) Despite the excellent tuning of the gun, the computer firing the gun sometimes failed to synchronize properly, so small static shifts occurred in the data. Therefore, the processing strategy was tailored to minimize the problems associated with data acquisition and to enhance the signal-to-noise ratio of the basement reflections as well as the increased temporal resolution of internal reflections.

Acknowledgments

I thank D.R. Hutchinson and C.W. Poag for providing the map for Chesapeake Bay Cruise 1996 and relevant information for data processing. I thank J.J. Miller and W.F. Agena for helping to improve the clarity of the paper.

Data Processing

The processing flowchart is shown in figure 2. As indicated in figure 2, the processing steps for the water gun data are slightly different from those of the air gun data.

Air Gun (GI Gun) Data

Static Correction and Direct Arrival Correction

As mentioned in the Introduction, inaccurate computer firing of the gun introduced a small static shift in the data. The shifts were measured visually on the screen display and were corrected to align the zero-time.

The offset between the GI gun and the center of the streamer was 50 m, and direct arrivals to the streamer interfered with reflections from the shallow water bottom. To suppress the direct arrival, we tried subtracting the running sum of 10 direct arrivals from the data. Figure 3*A* shows the original raw data with automatic gain control (AGC); figure 3*B* shows the same data after deconvolution (to be mentioned later) and suppression of direct arrivals. Strong arrivals in the beginning of the section in figure 3*A* are direct arrivals superimposed with weak reflections. Although these direct arrivals were reduced in figure 3*B*, the process did not enhance any interpretable shallow reflections. Therefore, we did not attempt to suppress direct arrivals in this processing.

Gain, Deconvolution

Because the primary concern in the data processing was to map the basement structure, preserving relative amplitudes was

Figure 1. Location map of the single channel seismic lines in Chesapeake Bay acquired in 1996. Line 3a and line 15a were shot using a water gun energy source; all other lines were shot using a GI gun (air gun) energy source.

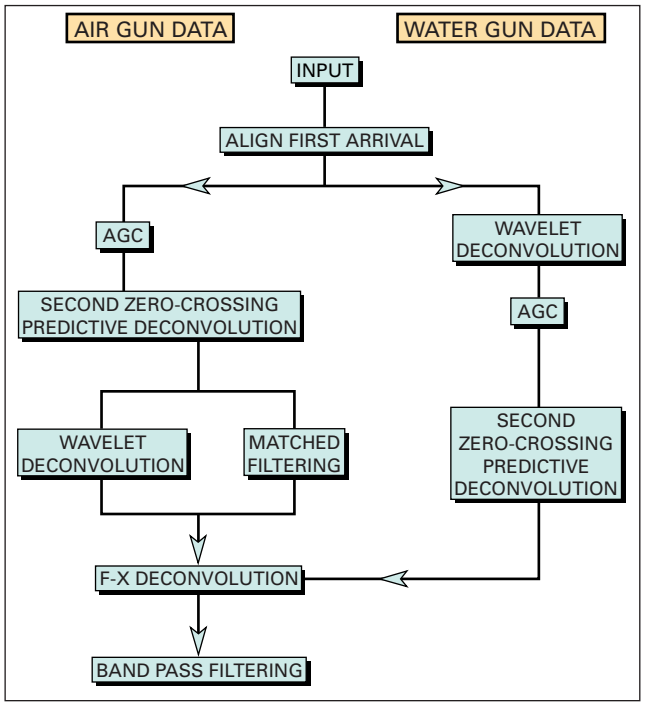

Figure 2. Processing flowchart. AGC, automatic gain correction.

not considered important. Therefore using an AGC with a 150 ms (millisecond) window is acceptable for the gain function. The raw data with the 150 ms AGC are shown in figure 3*A*.

Figure 3*A* reveals strong reverberations, particularly between 200 and 400 ms. Also tails of strong basement reflections near 520 ms due to the ringing of the air gun wavelet are evident in the seismic section. In order to suppress these reverberations, second zero-crossing deconvolution was applied. Second zero-crossing deconvolution is a type of predictive deconvolution where the prediction distance is the second zero-crossing of the auto-correlation of the trace. A single window with 120 ms or 180 ms operator length was used. The reason for using second zero-crossing deconvolution instead of spiking deconvolution comes from the consideration of signal-to-noise ratio as well as suppressing wavelet ringing in the processing.

The result of applying predictive deconvolution is shown in figure 3*B*. As indicated in this view, most of the reverberations were suppressed and the ability to interpret primary reflections was significantly enhanced.

Wavelet Deconvolution and Matched Filtering

To further improve temporal resolution and to correct the phase of the wavelet (ideally resulting in a zero-phase wavelet),

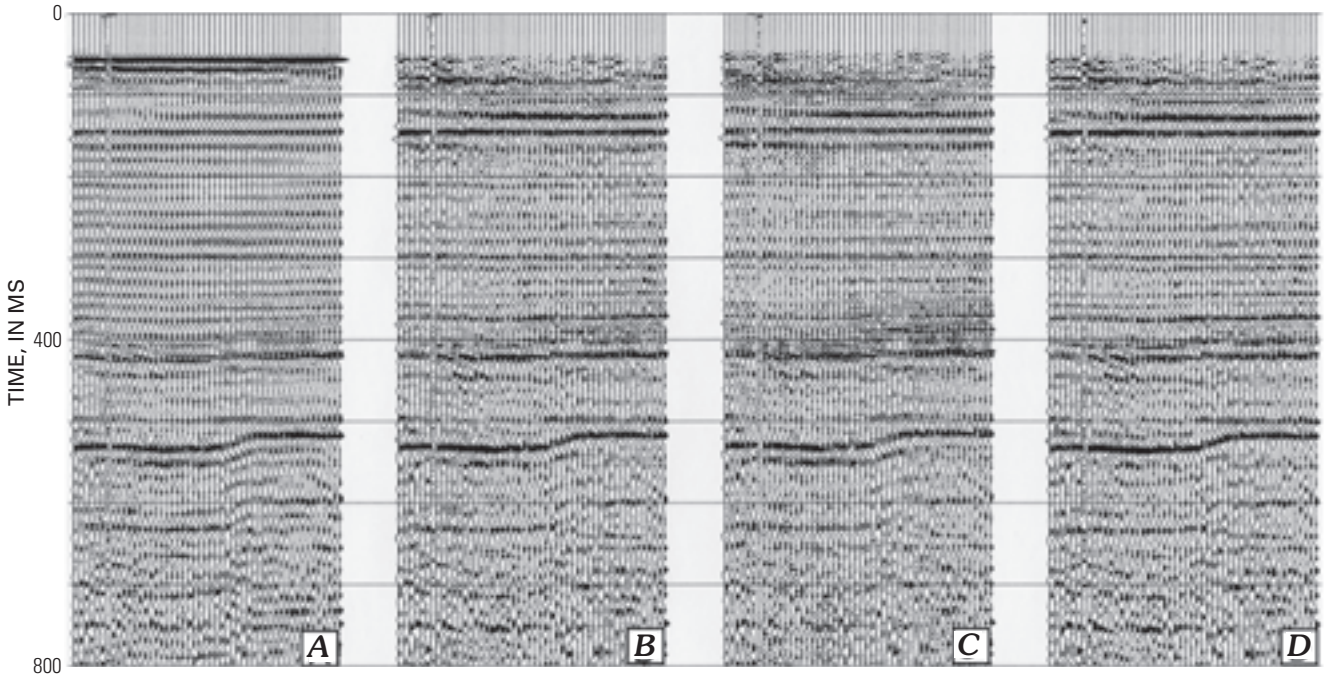

Figure 3. Examples of seismic data processing. *A*, Raw data with automatic gain correction applied. *B*, Result with a second zero-crossing deconvolution applied to data shown in *A*. *C*, Result with a wavelet deconvolution applied to data shown in *B*. *D*, Result with a matched filter applied to data shown in *B*.

a variable norm deconvolution method by Gray (1979) was used in the processing. This aids in the interpretation of internal disruptions of stratigraphy. About 300 random windows (window length is about 16 ms or 18 ms) were selected between about 150 and 450 ms in the deconvolved data, and wavelets were estimated using different norms, window lengths, and design areas. Deconvolved outputs were compared visually, and optimum parameters were chosen. A single deconvolution operator was derived from the optimum parameters and applied to the whole line.

Figure 3*C* shows an example of this wavelet deconvolution process for the data shown in figure 3*B*. Comparing figure 3*C* with figure 3*B* indicates that the wavelet processing increased the overall temporal resolution of the data. Notice the sharp reflections between about 350 ms and 550 ms in figure 3*C*. However, the continuity and strength of the basement reflections (reflections near 500 ms) are somewhat degraded in figure 3*C*. Therefore wavelet deconvolution is not an optimum processing method for the enhancement of basement reflections, so we used a matched filtering for the enhancement of the basement reflections. This approach can be easily understood if a simple convolution model for the reflection seismogram is employed.

The reflection seismogram can be approximated in the following simple convolution model:

$$S(t) = W(t)^{*}R(t) + N(t) \qquad (1)$$

where $S(t)$: seismogram,

$W(t)$: wavelet,

$R(t)$: reflectivity of the medium and assumed to be a random white sequence,

$N(t)$: noise, which is assumed to be random and uncorrelated with $R(t)$,

$*$: a convolution operator

In equation (1), it is assumed that the reverberation is already suppressed.

The purpose of wavelet deconvolution is used to remove the wavelet effect in equation (1), so the wavelet deconvolved section $S_w(t)$ can be written as

$$S_w(t) = R(t) + N'(t) \qquad (2)$$

where $N'(t)$ is the random noise deconvolved with the wavelet. As can be seen from equation (2), the wavelet deconvolution increases the temporal resolution by removing the wavelet effect, and at the same time it may increase the random noise component because the noise component ($N(t)$) itself was deconvolved. This property is not optimum in mapping the low signal-to-noise ratio basement reflections. To overcome this shortcoming of the wavelet deconvolution, we applied the matched filtering to the data for the basement reflections.

Mathematically, this can be written as

$$S_m(t) = W(t)\otimes W(t)^{*}R(t) + W(t)\otimes N(t) \qquad (3)$$

where $S_m(t)$ is the output with a match filtering applied and $\otimes$ indicates a cross-correlation operator. As indicated in equation (3), the match filtering is a process that seismic data are cross-correlated with a wavelet (Claerbout, 1992), so that this processing method increases the spectral component of the wavelet. Also, the spectral component outside the wavelet is suppressed in the output. This is an excellent signal-to-noise ratio enhancement filter, because the matched filter is designed such that ideally the presence of a signal is indicated by a single large amplitude in the output (Robinson and Treitel, 1980).

Figure 3*D* shows the result of applying the matched filter to the section shown in figure 3*B*. Comparing views *B*, *C*, and *D*,

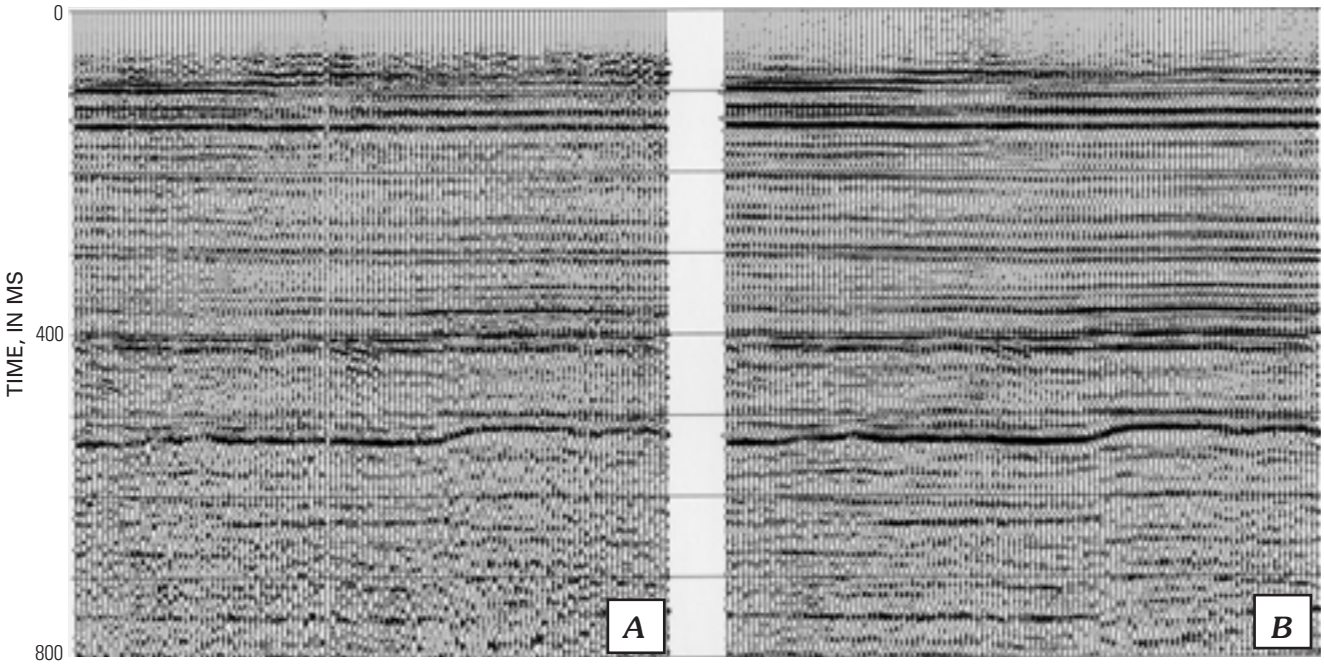

Figure 4. Example showing effect of signal enhancement filter (F-X deconvolution). *A*, Input (wavelet processed section). Portions of these data are shown in figure 3*C*. *B*, Result with the application of F-X filter. Filters were designed using eight traces and five time samples using complex Wiener filter.

we concluded that the matched filtering enhances basement reflections (events near 520 ms) for this line.

F-X Deconvolution

Common noise in the seismic section is random noise. To reduce this random noise, we used a F-X deconvolution method (Canales, 1984; Gulunay, 1986) as a final step of signal enhancement. This process uses the concept that the signal can be defined in terms of a simple model that separates the time and space variable, so that the signal can be formed by a sum of complex exponentials in the frequency-distance (F-X) domain. This is easily envisioned if we consider that arbitrary waves can be decomposed into many plane waves which can be predicted accurately in the F-X domain. To estimate the underlying signal, we implemented Wiener filter theory to derive a complex prediction filter using eight traces and five temporal samples. One of the advantages of the F-X deconvolution method is that the continuity of the reflections is improved without much smearing effect common to many mixing methods (for example, running sum).

Figure 4*A* shows a section without the application of F-X deconvolution, and figure 4*B* shows the result of F-X deconvolution applied to the data shown in view *A*. Notice that a noise trace in the middle of the section in figure 4*B* is substituted with signals predicted from the adjacent traces. In F-X deconvolution, an isolated trace is treated like random noise, because the single trace cannot be predicted in the F-X deconvolution (there is no spatial correlation). One of the concerns of applying multi-channel signal enhancement techniques is the reduction of spatial resolution due to the adverse mixing effect. Comparing reflection characters shown in figure 4, views *A* and *B*, clearly shows that the mixing effect is not problematic when using F-X deconvolution. Therefore, the processing strategy using F-X deconvolution would not hamper the ability of mapping faults, which is one of the primary concerns of data interpretation.

Water Gun Data

One difference in the data processing of air gun data and water gun data is the wavelet processing step. This is due to the fact that whereas the wavelet from the GI gun is nearly minimum phase and has a compact wave form, the wavelet from the water gun has a low-frequency precursor (Grow and others, 1986) and is a well-known mixed-phase wavelet. Variable norm deconvolution (Gray, 1979) can handle the mixed-phase wavelet, but these data presented difficulty in extracting a mixed-phased wavelet for the reasons described following.

In the air gun data processing, the wavelet deconvolution was applied after second zero-crossing deconvolution, and a wavelet was estimated from 300 random windows 16 or 18 ms long. This type of wavelet deconvolution using a random window works well for compact wave forms where there is no precursor, as demonstrated in Lee and others (1998). In the water gun data, the wavelet was extracted from the raw data using a fixed window, 34 ms long, and 300 traces. Even though the frequency content of water gun data is higher than that of the air gun data, a longer design window was used for the water gun data, because the precursor should be included in the wavelet extraction. The fixed window starts at 24 ms, near the onset of the precursor of the reflection.

Figure 5*A* shows the first 100 ms of water gun data without any gain correction. As indicated in the figure, directed arrivals (A-A′) and water bottom reflections (B-B′) interfere with each

other in such a way that the precursor of the reflection occurs between the precursor and main pulse of the direct arrival. Because of the interference of different wave types, extracting a reliable wavelet was difficult. The result of one of the many attempted wavelet deconvolutions is shown in figure 5*B*. In this case, direct arrivals were surgically muted to minimize the effect of mixing of the direct arrival with the water bottom reflections in the estimation of the water gun wavelet. The result shown in figure 5*B* indicates that the reflections near 40 ms are enhanced significantly and the interfering low-frequency tails near 50 ms in figure 5*A* were suppressed by the wavelet processing. At this stage, whether or not wavelet deconvolution was adequate for this data set is difficult to evaluate, but the advantage of the wavelet processing over predictive deconvolution can be drawn from the fully processed section.

Figure 6*A* shows the raw data with AGC; figure 6*B* shows the section processed using the method identical to the air gun data processing without wavelet deconvolution; and figure 6*C* shows the section processed using the wavelet processing described in this section. Figure 6*A* indicates the presence of much interference not only owing to the reverberatory nature of the reflections but also coming from the precursors of the reflections, so that interpreting the primary reflections is not easy. Figures 6*B* and 6*C* show significantly improved sections. However, as far as the clarity and continuity of the reflections are concerned, the result shown in figure 6*C*, processed with the wavelet deconvolution, shows better results than those shown in figure 6*B*, processed with the predictive deconvolution.

Discussion

Figure 7 shows the result of the processing of the air gun data for a portion of line 7, which was acquired using the GI gun. The result of minimal processing, AGC, and band pass filtering is shown in figure 7*A*, and the result of processing steps given in figure 2 with the application of matched filtering is shown in figure 7*B*. The strategy, using a second zero-crossing deconvolution and matched filtering, enhanced the basement reflections and suppressed the reverberatory energy for this line.

Because the bubble pulse is suppressed in the GI gun, the GI gun signature is clean as demonstrated in the first arrival event in figure 3*A*. However, the reverberatory nature of reflections due to the receiver ghosts, source ghosts, and water bottom multiples is evident in figure 3*A*. Therefore, for an accurate interpretation of internal disruptions of stratigraphy, deconvolution should be applied to the data. Considering the signal-to-noise ratio as well as the resolution of single channel data, we conclude that a predictive deconvolution with second zero-crossing predictive distance is optimum for this data set.

As mentioned previously, the effect of the direct arrival still remained in the processed section. In a conventional data set, the effect of direct arrivals interfering with the reflections is reduced, because the reflections usually arrive at a little later time. However, in this data set, the arrival times of direct and shallow reflections caused the waveforms to overlap. Instead of muting the first arrivals, we attempted a subtraction method (an average of 10 running sums of the direct arrivals was subtracted

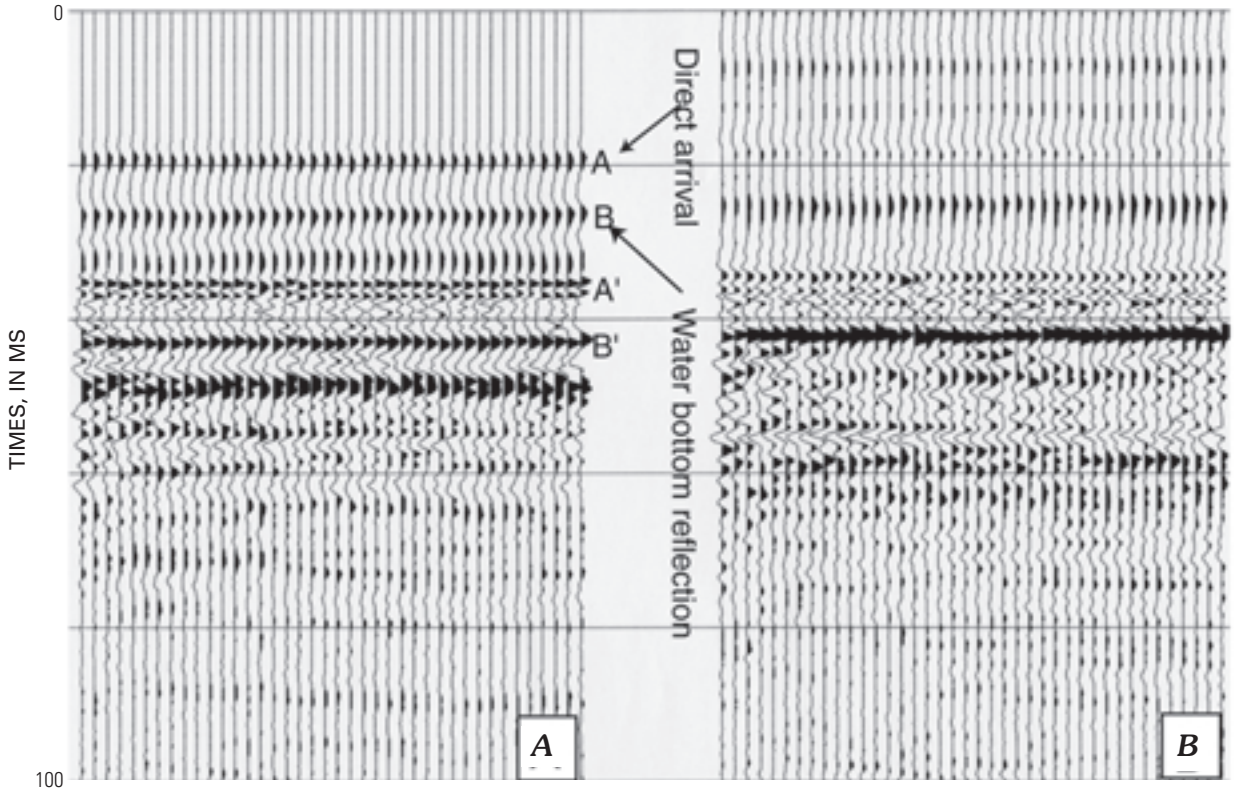

Figure 5. Example of wavelet deconvolution for the water gun data. Direct arrivals are denoted by A–A′ (A is the precursor and A′ is the main pulse of the direct arrival of the water gun signal); water bottom reflections are denoted by B–B′ (B is the precursor and B′ is the main pulse of the water bottom reflection). *A*, Raw water gun data. *B*, Water gun data after wavelet deconvolution.

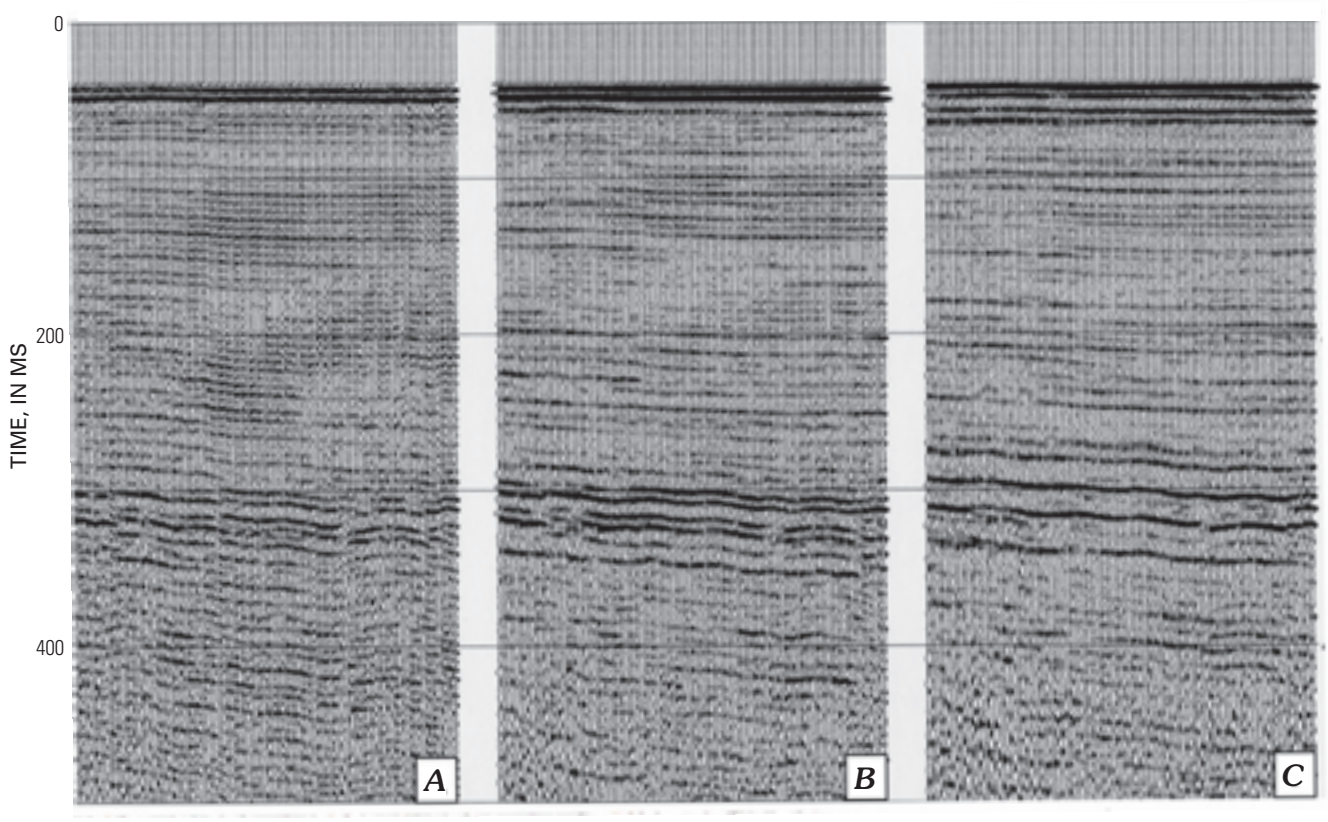

Figure 6. Example showing result of water gun data processing. *A*, Input with 100 ms AGC applied. *B*, Result of second zero-crossing deconvolution applied to data shown in *A* with F-X filtering application. *C*, Result of wavelet deconvolution with second zero-crossing deconvolution and F-X filtering applied to data shown in *A*.

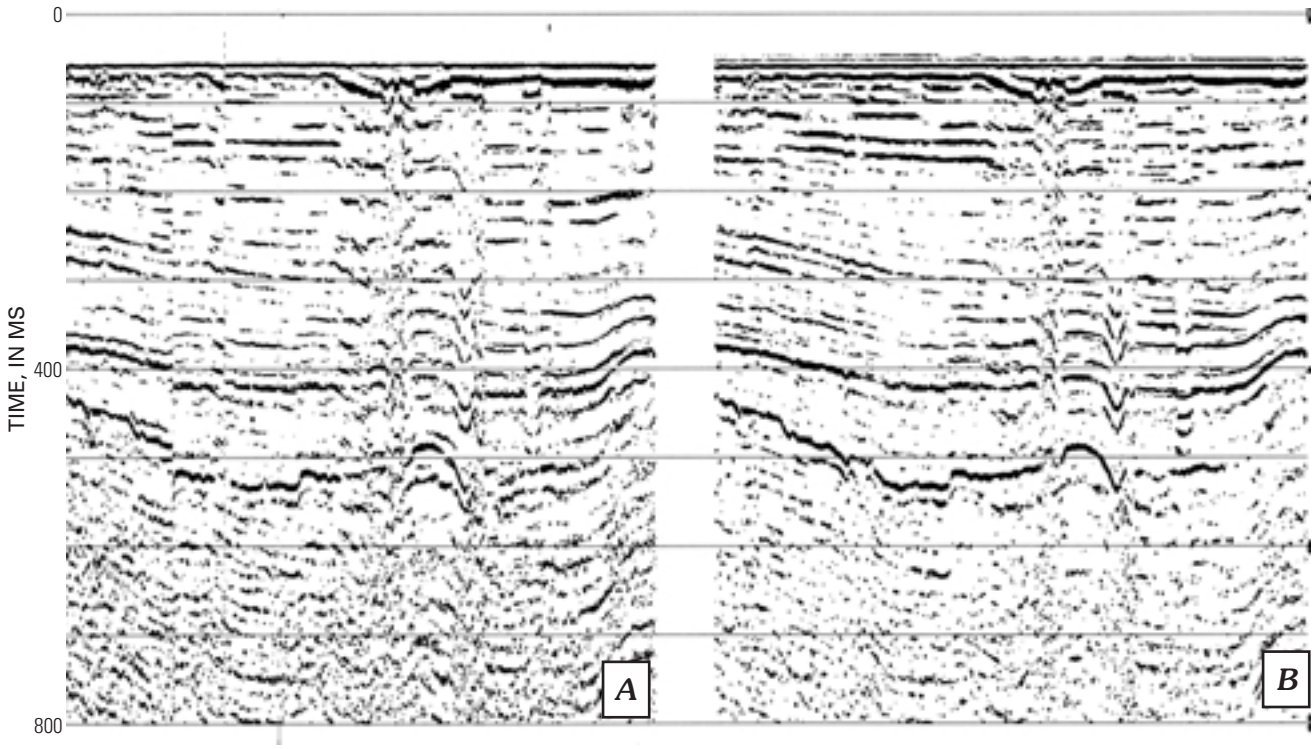

Figure 7. Examples of final processing for line 7, acquired by GI (air) gun. *A*, Raw data with AGC and band-pass filtering. *B*, Result with the processing steps shown in figure 2 applied.

from the seismic trace); the running sum was possible, because the water bottom reflection times between adjacent traces are nearly constant. However, this procedure did not perform well for this data set. Predictive deconvolution followed by a wavelet-processing scheme enhanced the shallow reflections slightly. The frequency shift toward lower frequencies owing to the presence of near-surface gas is somewhat compensated for by the deconvolution and wavelet processing.

The result of processing the water gun data shown in figure 6 implies that wavelet processing performed better than predictive deconvolution. However, one of the shortcomings of wavelet processing for this data set is the difficulty of extracting a reliable source signature because of interference of direct and reflected arrivals. The other drawback of wavelet processing of the water gun data is the problem associated with the application of the matched filtering. Because of the low-frequency precursor of the wavelet, the cross-correlation of wavelet with itself (matched filtering) results in three separate arrivals. Thus the output of the matched filtering looks much more complex than the input.

Summary

The employed processing steps shown in figure 2 provided enhanced seismic profiles for the interpretation of the impact structure and minimized the problems associated with the data acquisition. Increased temporal resolution and phase correction of the GI gun through the use of predictive deconvolution combined with wavelet deconvolution was found to be the optimum technique for improving the interpretability of the internal disruptions. On the other hand, the application of matched filter with predictive deconvolution was optimum in mapping the basement reflections due to the increased signal-to-noise ratio of the GI gun data.

For the water gun data set, applying wavelet deconvolution before predictive deconvolution may be better than applying predictive deconvolution, owing to the low-frequency precursor inherent to the water gun wavelet, but following the procedure this way has problems associated with the extraction of the wavelet and the application of wavelet matched filter.

References Cited

Canales, L.I., 1984, Random noise reduction: Society of Exploration Geophysicists 54th Annual International Meeting, Atlanta, Ga., Expanded Abstracts, p. 525–527.

Claerbout, J.F., 1992, Earth sounding analysis: Boston, Mass., Blackwell Scientific Publications, 304 p.

Gray, W.C., 1979, Variable norm deconvolution: Palo Alto, Calif., Stanford University Ph. D. thesis, 101 p.

Grow, J.A., Lee, M.W., Miller, J.J, Agena, W.F., Hampson, J.C., Foster, D.S., and Woellner, R.A., 1986, Multichannel seismic-reflection survey of KOA and OAK craters, *in* Folger, D.W., Sea-floor observations and subbottom seismic characteristics of OAK and KOA craters, Enewetak Atoll, Marshall Island: U.S. Geological Survey Bulletin 1678, p. D1–D46.

Gulunay, N., 1986, FXDECON and complex Wiener prediction filter: Society of Exploration Geophysicists 56th Annual International Meeting, Houston, Tex., Expanded Abstracts, p. 279–281.

Lee, M.W., Agena, W.F., Grow, J.A., and Miller, J.J., 1998, Seismic processing and velocity analysis: U.S. Geological Survey Open-File Report 98-34, 29 p.

Robinson, E.A., and Treitel, A., 1980, Geophysical signal analysis: Englewood Cliffs, N.J., Prentice-Hall, Inc., 468 p.